the radiated performance evaluation of multiple antenna reception and MIMO receivers, whose standardization is underway [1], [2].

Future research will cover the development of a measurement platform able to use several AUTs and to retrieve their radiation pattern (including phase), gain, efficiency, and MIMO parameters (as capacity, correlation and diversity gain) in an isotropic environment, with improved accuracy, and without the need of a three-dimensional positioning system, by performing mechanical stirring inside the RC.

REFERENCES

[1] 3rd generation partnership project, measurement of radiated performance for multiple input multiple output (MIMO) and multi-antenna reception for high speed packet access (HSPA) and LTE terminals (Release 11) 2012, 3GPP Tech. Rep. 37.976 v11.0.0.

[2] M. Á. García-Fernández, J. D. Sánchez-Heredia, A. M. Martínez-González, D. A. Sánchez-Hernández, and J. F. Valenzuela-Valdés, "Advances in mode-stirred reverberation chambers for wireless communication performance evaluation," *IEEE Commun. Mag.*, vol. 49, no. 7, pp. 140–147, Jul. 2011.

[3] A. Cozza and A. e.-B. A. El-Aileh, "Accurate radiation-pattern measurements in a time-reversal electromagnetic chamber," *IEEE Antennas Propag. Mag.*, vol. 52, no. 2, pp. 186–193, Apr. 2010.

[4] C. Lemoine, E. Amador, P. Besnier, J. Sol, J.-M. Floc'h, and A. Laisné, "Statistical estimation of antenna gain from measurements carried out in a mode-stirred reverberation chamber," in *Proc. XXXth URSI General Assembly and Scientific Symp.*, 2011, pp. 1–4.

[5] C. Lemoine, E. Amador, P. Besnier, J.-M. Floc'h, and A. Laisné, "Antenna directivity measurement in reverberation chamber from Rician K-factor estimation," *IEEE Trans. Antennas Propag.*, vol. 61, no. 10, pp. 5307–5310, Oct. 2013.

[6] C. Lemoine, E. Amador, and P. Besnier, "On the K-factor estimation for Rician channel simulated in reverberation chamber," *IEEE Trans. Antennas Propag.*, vol. 59, no. 3, pp. 1003–1012, Mar. 2011.

[7] V. Fiumara, A. Fusco, V. Matta, and I. M. Pinto, "Free-space antenna field-pattern retrieval in reverberation environments," *IEEE Antennas Wireless Propag. Lett.*, vol. 4, pp. 329–332, 2011.

[8] M. Á. García-Fernández, D. Carsenat, and C. Decroze, "Antenna radiation pattern measurements in reverberation chamber using plane wave decomposition," *IEEE Trans. Antennas Propag.*, vol. 61, no. 10, pp. 5000–5007, Oct. 2013.

[9] C. E. Shannon, "Communication in the presence of noise," *Proc. IRE*, vol. 37, no. 1, pp. 10–21, Jan. 1949.

[10] H. T. Friis, "A note on a simple transmission formula," *Proc. IRE*, vol. 34, no. 5, pp. 254–256, May 1946.

A Wideband Differential-Fed Slot Antenna Using Integrated Compact Balun With Matching Capability

Han Wang, Zhijun Zhang, Yue Li, and Zhenghe Feng

***Abstract*—This communication proposes a wideband differential-fed slot antenna that works in its dominant mode ($\lambda/2$ mode). The antenna has a near omnidirectional radiation pattern with vertical polarization, which is designed for near-ground wireless sensor node applications. A compact integrated T-slot balun and a loop to T-slot feeding structure are introduced to realize the differential feeding; the bandwidth is expanded to 30.7% (2.2 GHz–3.0 GHz) with a 3.8 dB peak gain. A detailed matching method without using lumped elements is proposed, which can be applied to various types of RFIC chips. A prototype is built and measured. Its differential impedance, antenna patterns, and gain are consistent with the simulation results.**

***Index Terms*—Antenna feeds, balun, impedance matching, slot antennas, wireless sensor networks.**

I. INTRODUCTION

Wireless sensor networks (WSN) are widely used in real-time monitoring applications. They are based on wireless sensor nodes that are built with RFIC chips. The differential RF interface can be observed in most of these chips. It can suppress external interference and ground noise and can double the output voltage to improve the output linearity and transmitting power effectively [1].

However, properly integrating these chips into a design is not a simple task. The differential (balanced) to single-ended (unbalanced) transition and the impedance matching are the main challenges that designers will confront with. Lumped element based balun [2], [3] and matching circuits [4] are the common solutions. Nevertheless, the size of the front-end expands with these interconnections, and the performance deteriorates due to their inherent insertion loss. Moreover, these solutions are not cost-effective, and the consistency of quality in mass production is hard to guarantee.

Based on this demand, differential-fed antennas designed for specific chips have become a new trend. This kind of antenna connects the chip directly with its differential port rather than by using a transition circuit [5]–[8]. Mature designs, such as the differential dipole, are widely adopted in RFIC designs [9], [10]. However, since their polarization directions are parallel to the ground, the wave does not propagate well when placed them near the wall or ground. For vertical polarization that is perpendicular to the ground, differential-fed patch antennas are the representative designs[11], [12] . Nevertheless, in near ground wireless sensor node applications, an omnidirectional radiation

Manuscript received October 30, 2013; revised February 28, 2014; accepted July 03, 2014. Date of publication July 25, 2014; date of current version October 02, 2014. This work was supported in part by the National Basic Research Program of China under Contract 2013CB329002, in part by the National High Technology Research and Development Program of China (863 Program) under Contract 2011AA010202, the National Natural Science Foundation of China under Contract 61271135, the China Postdoctoral Science Foundation funded project 2013M530046, and in part by the National Science and Technology Major Project of the Ministry of Science and Technology of China 2013ZX03003008-002.

The authors are with the State Key Lab of Microwave and Communications, Tsinghua National Laboratory for Information Science and Technology, Tsinghua University, Beijing, 100084, China (e-mail: zjzh@tsinghua.edu.cn).

Color versions of one or more of the figures in this communication are available online at http://ieeexplore.ieee.org.

Digital Object Identifier 10.1109/TAP.2014.2343238

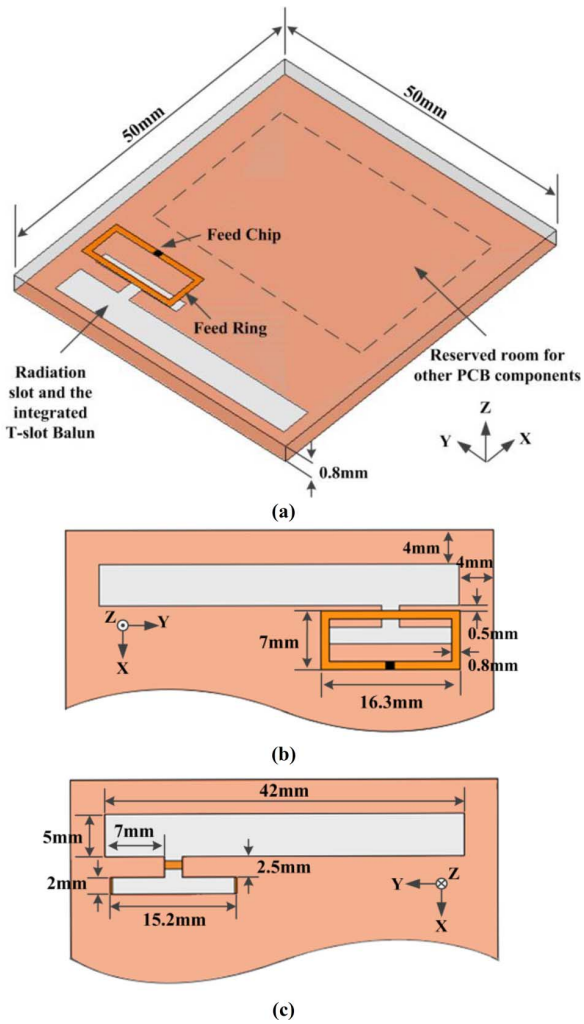

Fig. 1. The geometry of the proposed slot antenna.

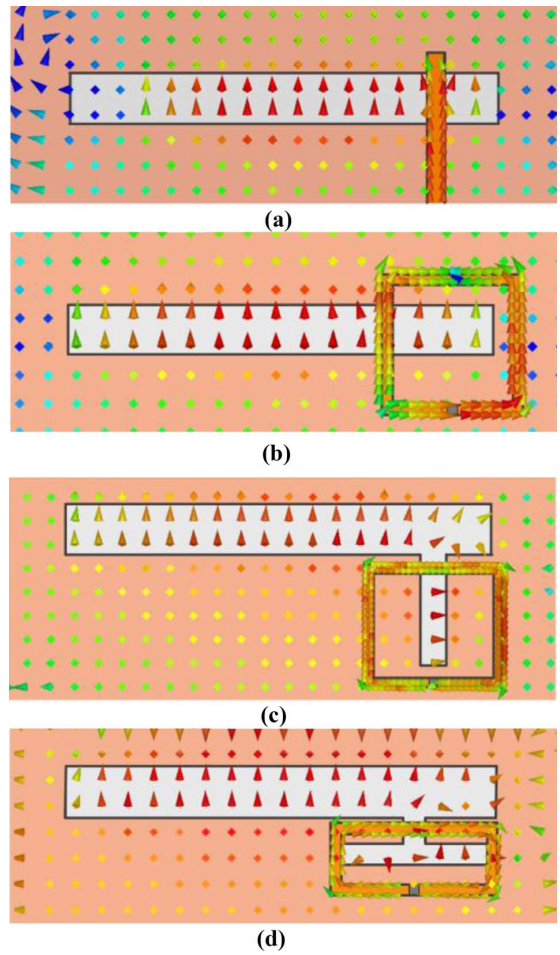

Fig. 2. The evolution of the proposed slot antenna (a) Microstrip feed slot (b) Loop directly feed (c) Loop to slot feed (d) Loop to T-slot feed.

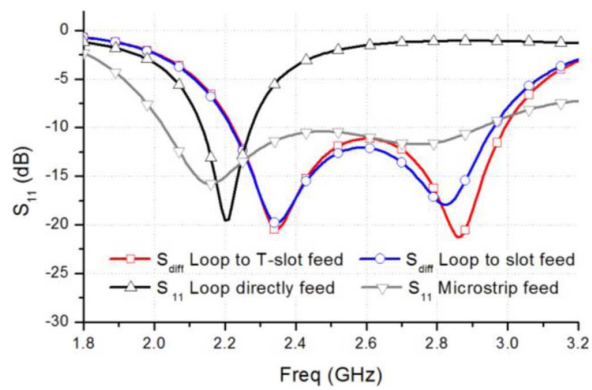

Fig. 3. Bandwidth comparisons among four types of slot antennas.

pattern is required for network grouping, which cannot be satisfied with the unidirectional radiation pattern of the patch. Comparatively, the slot antenna is a good candidate because it has a near omnidirectional and vertically polarized radiation pattern. However, the electric field generated by its dominant mode ($\lambda/2$ mode) is symmetric, which is difficult to be excited with a differential profile. In the existing research literature, only the slot working in the higher harmonic mode [13] is fed with a differential profile, which cannot satisfy the size requirement of the sensor node application.

In this communication, a wideband differential-fed slot antenna that works in its dominant mode is proposed and fabricated. A differential loop is applied to provide a differential port at the same position as in the traditional single-ended design. A T-slot balun is introduced to realize the differential to single-ended transition, and a dual resonant character is achieved by using this loop to T-slot feeding structure. The measurement results show that this design achieves a bandwidth of approximately 30% (2.2–3.0 GHz), with a 3.8 dB peak gain and a 2 dB average gain, which fully exploits the wideband character of the slot antenna. A detailed matching method is provided, which uses the adjustable geometric parameters in the radiation slot, T-slot balun, and the loop to T-slot transition. This design can be used extensively in wireless sensor node applications, especially for those who require a vertically polarized omnidirectional radiation pattern and a wideband character.

II. Mixed-Mode S-Parameters

In the single-ended design, a real ground exists and acts as the voltage reference when defining the S-parameters [14]. However, in the differential design, each terminal of the feeding structure can be viewed as a port, and both terminals carry the signals where no real ground exists. If the designer still treats the antenna as a single-ended structure by assigning one port as the signal and another as the ground, the definition of the S-parameters will remain valid if the feeding structure is symmetric. However, if the feeding structure is asymmetric, a common mode leakage will appear and the single-ended

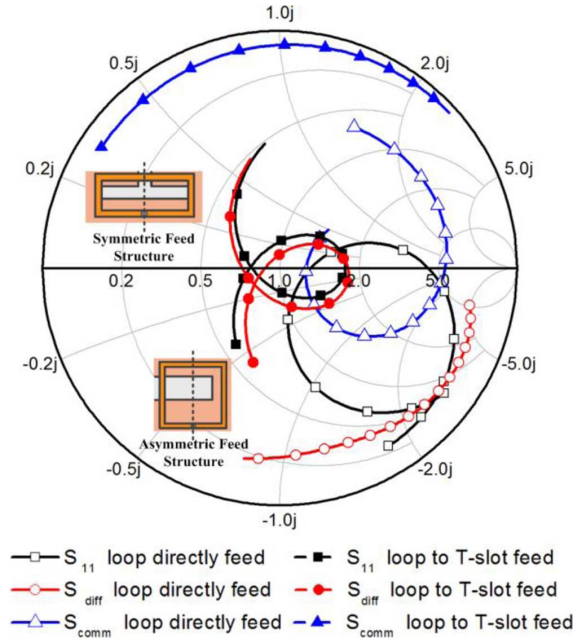

Fig. 4. The mixed-mode S-parameters comparison between the loop directly feed and loop to T-slot feed.

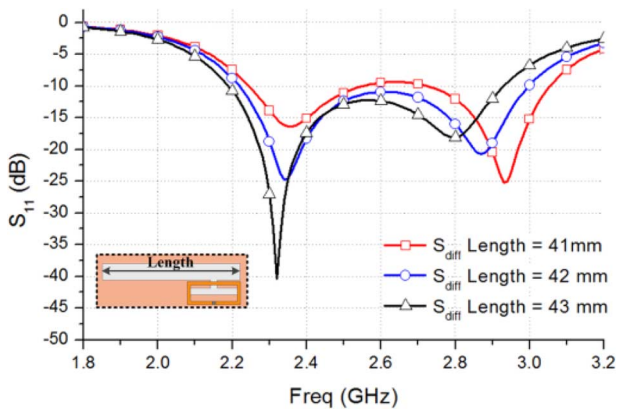

Fig. 5. The effect of tuning the length of the radiation slot.

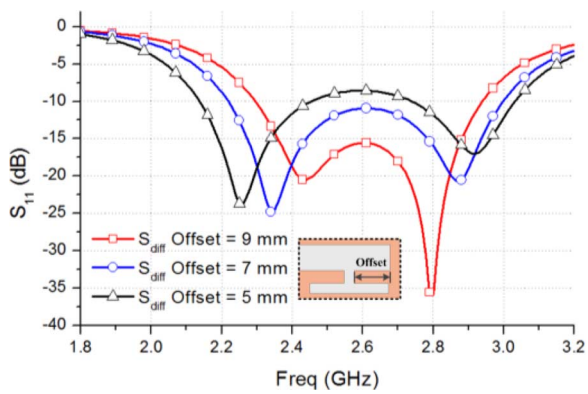

Fig. 6. The effect of tuning the T-slot along the radiation slot.

S-parameters will no longer be able to characterize its impedance. Thus, mixed-mode S-parameters [15] should be adopted instead to evaluate the impedance. These include two parameters, S_{diff} and S_{comm}, which can be calculated with (1), where S_{11}, S_{21}, S_{12}, S_{22},

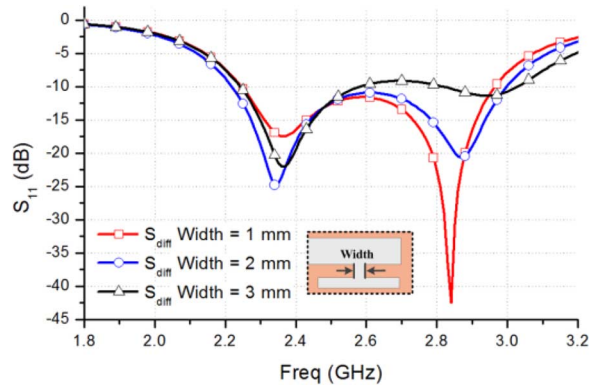

Fig. 7. The effect of tuning the width of the T-slot transition.

represent the conventional two-port S-parameters that are measured by viewing the differential port as a two-port structure.

$$S_{diff} = \frac{1}{2}(S_{11} - S_{21} - S_{12} + S_{22})$$
$$S_{comm} = \frac{1}{2}(S_{11} + S_{21} + S_{12} + S_{22}). \quad (1)$$

In the following sections, mixed-mode S-parameters are adopted to evaluate the antenna performance. The S_{11} refers to the single-ended S-parameters acquired by viewing the differential port as a single-ended structure; S_{diff}, S_{comm} refer to the mixed-mode S-parameters as defined in (1). The difference between S_{11} and S_{diff} can be used to reflect the symmetric character of the proposed feeding structure.

III. Antenna Design

The geometry of the proposed antenna is shown in Fig. 1, and the detailed dimensions are noted in Fig. 1(b) and (c). The antenna consists of a radiation slot, a T-slot balun, and a differential loop, which are fabricated on a square-shaped double sided FR-4 ($\varepsilon_r = 4.4, \tan\delta = 0.02$) based printed circuit board (PCB).

In the traditional single-ended design, a microstrip line is placed across one side of the slot, which can generate the dominant mode of the slot as shown in Fig. 2(a). To achieve the differential to single-ended transition without changing its working mode, an intuitive way is to replace the microstrip line in the single-ended design with a differential loop as shown in Fig. 2(b). Nevertheless, the S-parameters shown in Fig. 3 indicate that this is a narrowband solution. Moreover, the symmetric character of the feeding structure depends largely on the feeding position. When the loop is fed at the original (single-ended design) position that located at the bottom of the slot, the current on the loop is unbalanced as shown in Fig. 2(b). The mixed-mode S-parameters show a large difference from the single-ended S-parameters as shown in Fig. 4, which indicates that the feeding structure is asymmetric and the differential mode is not matched in this case.

To achieve the symmetric feeding and generate the dominant mode, this communication proposes an integrated slot to slot balun and its variation, a T-slot to slot balun, as shown in. Fig. 2(c) and (d). By placing the differential loop right above the integrated balun, the current on the loop is balanced as shown in Fig. 2(c) and (d), and the differential mode is matched as shown in Fig. 4. The feeding structure becomes symmetric, which can be verified by the minor difference between S_{11} and S_{diff} as shown in Fig. 4.

Moreover, the loop-to-slot transition introduces more adjustable geometric parameters into this design. It adds additional distributed

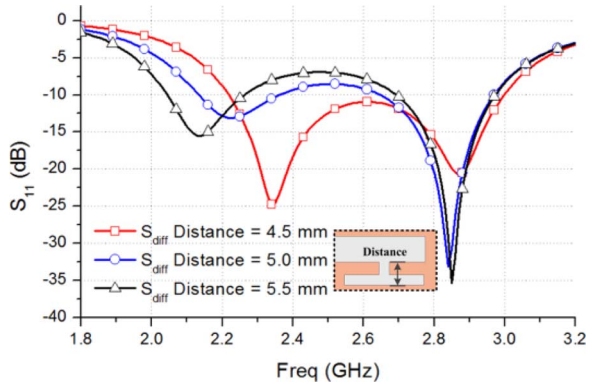

Fig. 8. The effect of tuning the distance of the T-slot's upper branch.

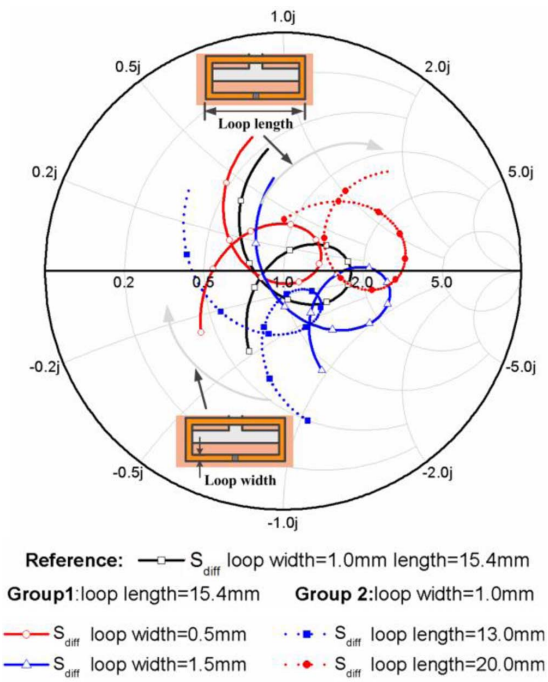

Fig. 9. The effect of tuning the length and the width of the feeding loop.

elements to produce dual-resonance as shown in Fig. 3. This expands the bandwidth effectively. Around 30.7% (2.2–3.0 GHz) bandwidth is achieved in the simulation, which is comparable to that in the single-ended slot design.

Since the loop to T-slot design occupies a smaller area on the PCB and the reversed current in the T-slot has a minor effect on the polarization of the antenna, it is adopted as the final design.

IV. Impedance Matching and Parameter Study

Impedance matching is the most important aspect in the RFIC based antenna design. To offer optimal performance, the impedance of the antenna should directly match the complex conjugate of the chip impedance. In this design, by tuning the radiation slot, the T-slot balun, and the differential loop together, differential impedance matching can be achieved for various types of RFIC chips. The design principle is described as follows.

A. The Radiation Slot

The radiation slot is a rectangular slot etched on the ground of the PCB. Its equivalent electrical length determines the resonant frequency,

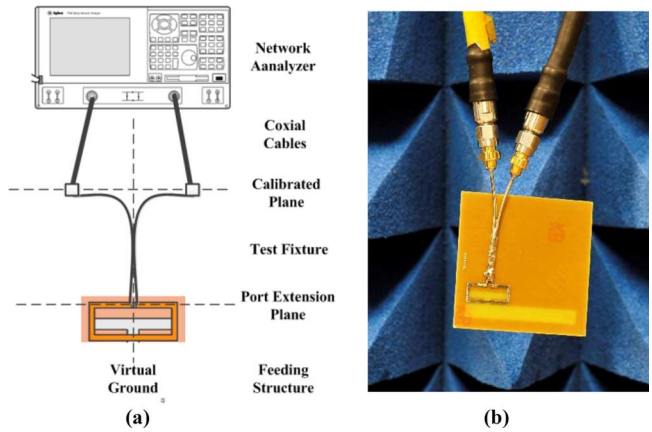

Fig. 10. The measurement scheme and the prototype under test (a) Test Scheme (b) Antenna Under Test.

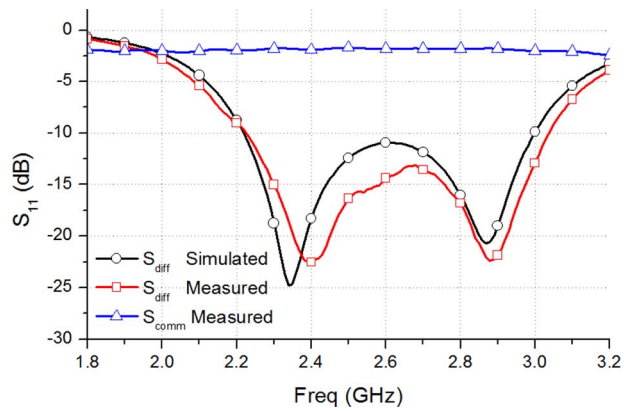

Fig. 11. The simulated and measured mixed-mode S-parameters.

which can be tuned by changing the length/width of the radiation slot and the permittivity of the substrate. Fig. 5 shows the relationship between the resonant frequency and the length of the radiation slot.

B. The T-Slot Balun

The T-slot balun achieves the balanced to unbalanced transition from the differential loop to the radiation slot. By shifting the T-slot along the radiation slot as shown in Fig. 6, the input impedance of the radiation slot changes, affecting the resonant character of the antenna as a whole. For individual resonant peaks, the resonant frequency and resonant depth can be tuned separately. Figs. 7 and 8 show the tuning process that is done by changing the width of the T-slot and the distance from the upper branch of the T-slot to the radiation slot.

C. The Differential Loop

The differential loop provides a differential port to the chip and couples the field into the T-slot balun. Two parameters, namely the length and width of the loop, can be used to achieve the orthogonal movement of the impedance trace on the Smith chart as shown in Fig. 9. Thus, the loop can be fitted into different impedance centers on the Smith chart as required in conjugate matching, which can be applied to different chips without using lumped elements.

By properly tuning and combining these three parts together, the proposed antenna can achieve conjugate matching for different chips and resonant frequencies. The elimination of lumped elements lowers the cost and improves the consistency of quality in mass production. Meanwhile, better performance and lower insertion loss are achieved, which

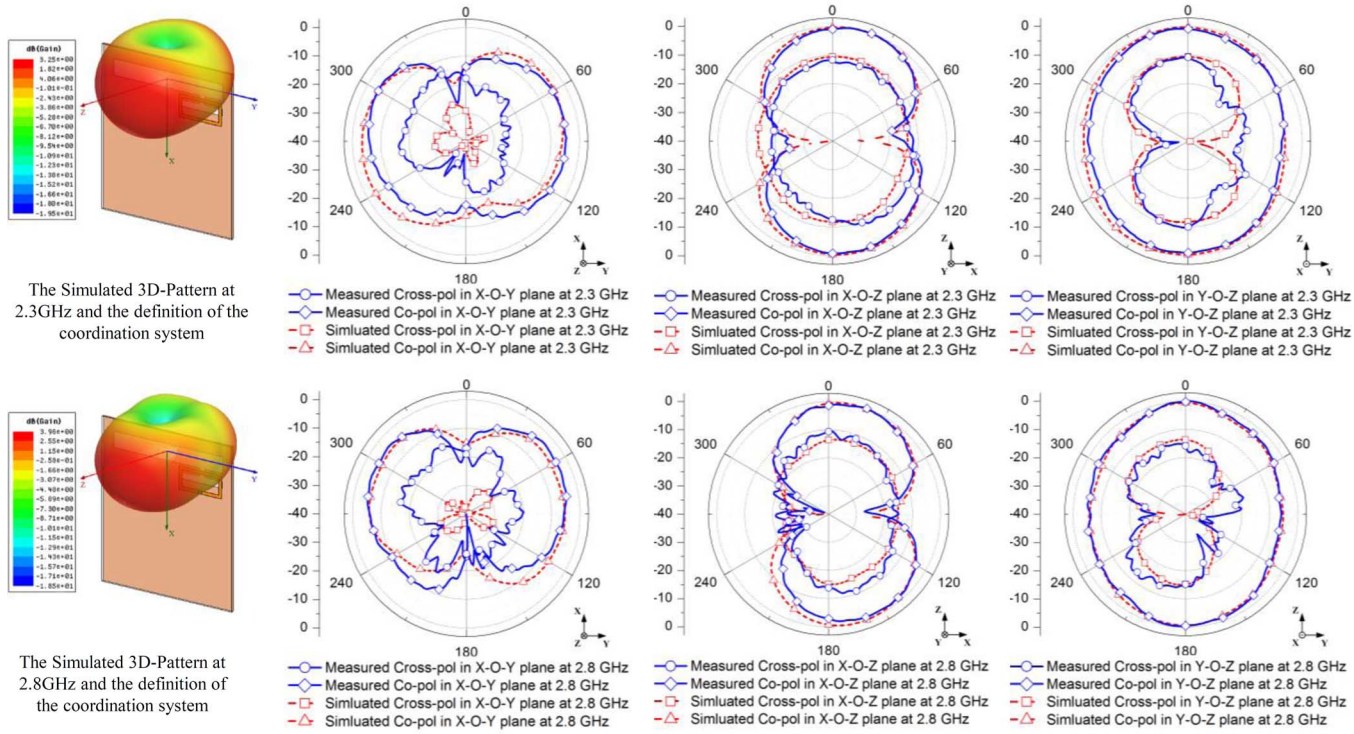

Fig. 12. The simulated and measured radiation patterns of the proposed antenna.

makes the antenna more useable and reliable in wireless sensor network applications.

V. Prototype and Measurement

With the geometry shown in Fig. 1, a prototype is fabricated and shown in Fig. 10(b). For verification purpose, the differential impedance is designed as 50 Ohms. Relative parameters, including differential impedance, radiation pattern, and gain, are measured to validate its performance.

A. Differential Impedance

The differential impedance is measured with a differential probe as shown in Fig. 10 [16]. The probe is a symmetric two-port fixture built with two semi-rigid coaxial cables. The Agilent VNA E5071B, along with the E-Cal Module 85097B, is used to perform the test. Fig. 10(a) shows the measurement setup, which is conducted in a chamber environment with the following steps:

1) Connect two coaxial cables to the VNA; use the E-Cal module to calibrate the measuring plane to the ports of the cables.
2) Attach the fixture to the cables, short the central conductor to the outer conductor, and perform a "short type" port-extension to calibrate the measuring plane to the ports of the fixture.
3) Connect the antenna to the fixture, perform the measurement, and save the results.

As shown in Fig. 11, the measured differential impedance matches the simulation result well, and the common mode leakage is almost negligible. A slight shift in frequency can be observed in the result, which may be attributed to fabrication errors or variations in the permittivity of the PCB substrate.

B. Antenna Patterns

The antenna patterns are measured in an ETS anechoic chamber AMS8500. Fig. 12 shows the measured patterns in comparison with the simulation results at 2.3 GHz and 2.8 GHz. The simulated 3D patterns are also provided as coordination system reference. It can be observed that the measured patterns fit the simulation results well, and a near omnidirectional radiation pattern in the Y-O-Z plane is achieved as expected.

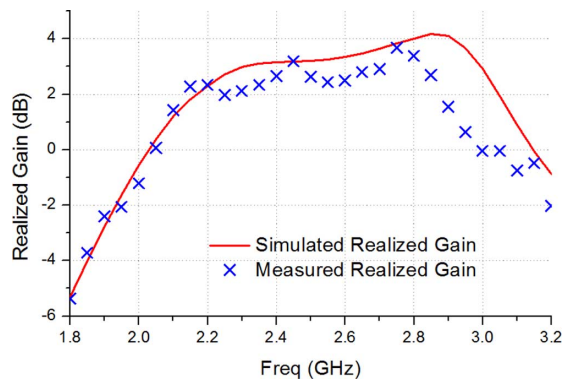

Fig. 13. The simulated and measured gain of the proposed antenna.

C. Gains

The gain, which is also measured in the ETS anechoic chamber, shows the same trends as the simulation result shown in Fig. 13. The peak gain reaches 3.8 dB at 2.75 GHz, and the average gain remains above 2 dB from 2.2 GHz to 2.9 GHz.

VI. Conclusion

In this communication, a differential-fed slot antenna that works in its dominant mode $(\lambda/2)$ is proposed and fabricated. This design fills the gap in mature differential designs (dipole, patch, etc.) and provides a near omnidirectional, vertically polarized radiation pattern. By introducing a compact integrated T-slot balun and a loop to T-slot transition, this design achieves the balanced to unbalanced transition and expands the bandwidth effectively. A bandwidth of approximately 30.7% is achieved and the average gain remains above 2 dB. A matching

method is proposed without using lumped elements, which can be applied to various types of RFIC chips in sensor node applications.

REFERENCES

[1] R. Bourtoutian, C. Delaveaud, and T. Serge, "Differential antenna design and characterization," in *Proc. 3rd Eur. Conf. Antennas Propag.*, 2009, pp. 2398–2402.

[2] W. Bakalski, W. Simbürger, H. Knapp, H. Wohlmuth, and A. L. Scholth, "Lumped and distributed lattice-type LC-Baluns," in *Proc. IEEE MTT-S Int. Microwave Symp. Dig.*, 2002, pp. 209–212.

[3] V. Gonzalez-Posadas, C. Martin-Pascual, J. L. Jiménez-Martín, and D. Segovia-Vargas, "Lumped-element balun for UHF UWB printed balanced antennas," *IEEE Trans. Antennas Propag.*, vol. 56, no. 7, pp. 2102–2107, Jul. 2008.

[4] Z. J. Zhang, *Antenna Design for Mobile Devices*. Hoboken-Piscataway, NJ, USA: Wiley-IEEE Press, 2011, pp. 25–28.

[5] K. M. Chan *et al.*, "Differential aperture coupling technique for passive and active integrated antenna design," *IET Microw. Antennas Propag.*, vol. 1, no. 2, pp. 458–464, Apr. 2007.

[6] Z. Duan, Y. X. Guo, R. F. Xue, M. Je, and D. L. Kwong, "Differentially fed dual-band implantable antenna for biomedical applications," *IEEE Trans. Antennas Propag.*, vol. 60, no. 12, pp. 5587–5595, Dec. 2012.

[7] T. Brauner, R. Vogt, and W. Bachtold, "A differential active patch antenna element for array applications," *IEEE Microw. Wireless Compon. Lett.*, vol. 13, no. 4, pp. 161–163, Apr. 2003.

[8] M. J. Li and K.-M. Luk, "A differential-fed magneto-electric dipole antenna for UWB applications," *IEEE Trans. Antennas Propag.*, vol. 61, no. 1, pp. 92–99, Jan. 2013.

[9] D. Puente, J. I. Sancho, J. García, J. De No, J. Gomez, and D. Valderas, "Matching radio frequency identification tag compact dipole antennas to an arbitrary chip impedance," *IET Microw. Antennas Propag.*, vol. 3, no. 4, pp. 645–653, Jun. 2009.

[10] K. M. Chan, E. Lee, P. Gardner, and P. S. Hall, "A differentially fed electrically small antenna," in *Proc. IEEE AP-S Int. Symp.*, Jun. 2007, pp. 2447–2450.

[11] Y. P. Zhang, "Design and experiment on differentially-driven microstrip antennas," *IEEE Trans. Antennas Propag.*, vol. 55, no. 10, pp. 2701–2708, Oct. 2007.

[12] S. V. Hum and H. Y. Xiong, "Analysis and design of a differentially-fed frequency agile microstrip patch antenna," *IEEE Trans. Antennas Propag.*, vol. 58, no. 10, pp. 3122–3130, Oct. 2010.

[13] L. Li, J. Yang, X. W. Chen, X. W. Zhang, R. B. Ma, and W. M. Zhang, "Ultra-wideband differential wide-slot antenna with improved radiation patterns and gain," *IEEE Trans. Antennas Propag.*, vol. 60, no. 12, pp. 6013–6018, Dec. 2012.

[14] D. M. Pozar, *Microwave Engineering*, 3rd ed. New York, NY, USA: Wiley, 2005, pp. 174–183.

[15] D. E. Bockelman and W. R. Eisenstadt, "Combined differential and common-mode scattering parameters: theory and simulation," *IEEE Trans. Microw. Theory Techn*, vol. 43, no. 7, pp. 1530–1539, Jul. 1995.

[16] X. Qing, K. G. Chean, and Z. N. Chen, "Impedance characterization of RFID tag antennas and application in tag co-design," *IEEE Trans. Microw. Theory Tech.*, vol. 57, no. 5, pp. 1268–1274, May 2009.

Long Slots Array Antenna Based on Ridge Gap Waveguide Technology

Mohamed Al Sharkawy and Ahmed A. Kishk

***Abstract*—Ridge gap waveguide (RGW) technology is used in the design of a frequency scanning antenna with high gain and directivity. A Quasi-TEM horn with shaped ridge is designed as a guiding structure between two metallic surfaces. The waves are suppressed beyond the shaped ridge area between the metallic surface and the artificial magnetic conductor (AMC); realized by a bed of conducting nails. The ridge is shaped to generate uniform field distribution in the enclosed air gap. Non-resonance radiating long slots are introduced in the top metallic layer. Since the slots are separated by a guiding wavelength, a grating lobe in the visible region exists. The structure is built and tested. Good agreement between measured and simulated results is obtained with an average gain of 14.5 dBi within a bandwidth of 22%. To reduce the grating lobe, two different techniques are proposed. These techniques achieve a reduction in the grating lobe and enhance the antenna gain to an average gain of 18.5 dBi.**

***Index Terms*—Beam scanning, h-plane horn antenna, linear slots, ridge gap waveguide, uniform field distribution.**

I. INTRODUCTION

Recently, researchers have been interested in the applications at the high frequency range due to the fast evolution of wireless systems that triggered the need of higher data rates and bandwidths. When dealing with applications at the high frequency range, one should consider the high losses introduced due to higher operating frequencies. Thus, low loss components are needed. Microstrip technology has been considered to be the most popular planar technology used for wide range of applications. However, it suffers from the high losses introduced due to the presence of dielectric material as well as the radiation losses [1], which affect the structure efficiency. A new gap waveguide technology has been recently introduced, which depends only on metallic structures that would be suitable for high frequencies due to their low losses [2]–[4]. The idea of this technology is to introduce a propagating wave in a narrow gap guided by two parallel metallic plates; one of them would be a guided ridge [4]. In order to prevent the parallel plate modes from propagating away from the ridge area, an artificial magnetic conductor (AMC), in a sense, should be introduced in the bottom plate leaving an air gap from the top. This artificial magnetic conductor as illustrated in [4]–[6] can be implemented by periodic bed of conducting pins that have a specific cut-off band.

Different kinds of applications have been studied and investigated using the ridge gap waveguide (RGW) technology. Due to its low losses, it will be widely used for applications at the millimeter and sub millimeter range of frequencies. It has been used in the design of microstrip filters [7], couplers and MMIC technology [8], power dividers [9], and rat race balun [10]. Moreover, researchers have

Manuscript received December 09, 2013; revised June 13, 2014; accepted July 23, 2014. Date of publication August 05, 2014; date of current version October 02, 2014.

M. Al Sharkawy is with Concordia University, Electrical and Computer Engineering Department, Montreal, Canada and also with the Arab Academy for Science, Technology, and Maritime Transport, Alexandria, Egypt (e-mail: msharkawy@aast.edu).

A. A. Kishk is with Concordia University, Electrical and Computer Engineering Department, Montreal Canada (e-mail: kishk@encs.concordia.ca).

Color versions of one or more of the figures in this communication are available online at http://ieeexplore.ieee.org.

Digital Object Identifier 10.1109/TAP.2014.2345411